

# A toroidal sector for the electron branch of a reaction microscope

X Wang<sup>1,2,4</sup> and S Hagmann<sup>2,3</sup>

<sup>1</sup> Shanghai EBIT Laboratory, Institute of Modern Physics, Fudan University, Shanghai 200433, People's Republic of China

<sup>2</sup> GSI, Darmstadt, Germany

<sup>3</sup> Institut für Kernphysik, University of Frankfurt, Germany

<sup>4</sup> The Key Laboratory of Applied Ion Beam Physics, Ministry of Education, People's Republic of China

Received 26 July 2006, in final form 18 October 2006

Published 30 November 2006

Online at [stacks.iop.org/MST/18/161](http://stacks.iop.org/MST/18/161)

## Abstract

We present calculations for the electron branch of a reaction microscope with a toroidal magnetic field for experiments in a storage ring. A suitable toroidal magnetic field guides the electrons away from the vicinity of the coasting beam onto a 2D position-sensitive detector. Other than in the linear geometry, 2D position and time-of-flight information for electrons on the detector are coupled in this geometry. For beam velocities below 12 au corresponding to projectile specific energies  $\leq 3.6$  AMeV fast electrons emitted by the projectile and slow electrons can still conveniently be mapped simultaneously onto a single electron detector. For a position and time resolution of 0.2 mm and 1 ns, respectively, 1 eV can be resolved for electrons of 200 eV, which corresponds to a momentum resolution of about 0.3 au. A prototype for the toroidal sector will be tested using Unilac beams.

(Some figures in this article are in colour only in the electronic version)

## 1. Introduction

Investigations of the stationary structure of atoms or ions have traditionally been central to research activities in atomic physics. Precise information on the binding energies of electrons and thus on the atomic structure is needed for the understanding of fundamental questions of atomic physics. An impressive agreement has been achieved between experiment and QED theory, e.g. for the energy levels of heavy few-electron ions, the 1s Lamb shift in hydrogen and the electronic  $g$  factor of H-like  $O^{7+}$  [1–3].

However, dynamical many-body systems, e.g. a complete description of target and projectile ionization, still present a redoubtable challenge for theory and experiment. Rapid progress in this field was stimulated since localized gas-jet targets combined with RIMS (recoil ion momentum spectroscopy) were implemented successfully [4, 5]. An exhaustive and detailed review of the evolution of kinematically complete experiment techniques leading to the reaction microscope is given in [6]. Here we give a brief overview of aspects pertinent to the context of the current work.

Recoil ions created in the reaction region are extracted by an electrostatic field and projected onto a 2D position-sensitive detector. By measuring TOF (the time-of-flight) and the position of the ions on the detector, the complete initial momentum vector of the recoil ion can be calculated. A solid angle of nearly  $4\pi$  is achieved for the recoil ions in this way. Internally cold supersonic gas jets provided a great advance in momentum resolution, corresponding energy resolutions far below 1 meV were realized, that is a momentum of 0.7 au for helium ions. This enabled studies of atomic collisions with momentum transfers down to below 1 au. Precooling of the target gas before the supersonic expansion pushed the resolution to  $\Delta E_R \sim 30 \mu\text{eV}$  for helium ions and thus was termed cold-target recoil-ion momentum spectroscopy (COLTRIMS) [8–10]. The combination of a high-resolution recoil-ion momentum spectrometer with a novel low-energy electron analyser where the basic principles of recoil-ion detection are now applied in addition to the electrons forms the so-called reaction microscope [11]. Using a combination of electrostatic extraction fields with solenoidal magnetic fields, for the first time the kinematically complete momentum vectors of all reaction products are determined, with a

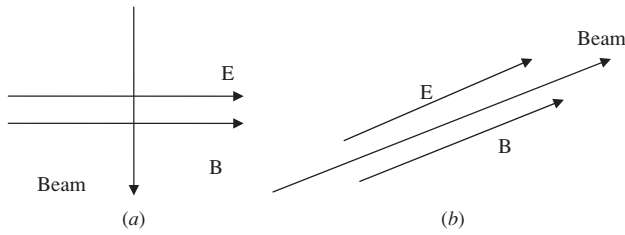


**Figure 1.** Top view of beam and electric and magnetic fields for (a) transverse reaction microscope, (b) longitudinal reaction microscope.

recoil-ion momentum resolution of a few per cent of an atomic unit and a solid angle of nearly 100% of  $4\pi$  [11, 12]. Using these or similar ‘reaction microscopes’, kinematically complete experiments have been performed [5, 7]. The solid angle  $d\Omega \approx 4\pi$  for both electrons and recoiling ions, exceeds the solid angle of standard configurations by more than an order of magnitude.

Recently, a significant further reduction of the target temperature has been achieved when laser-cooled atoms trapped in a magneto-optical trap (MOT) were used as a target. A momentum resolution of  $\Delta P_R = 0.003$  au for lithium and  $\Delta P_R = 0.01$  au for rubidium is achieved. Many experiments have been done during the past 5 years [13–18]. See [5] for an extensive review of recent progress in the field.

In the study of ion–atom collisions reaction microscopes have so far only been used in single-pass experiments, as storage ring environments present a formidable challenge for a longitudinal configuration reaction microscope with large area detectors positioned in proximity to the coasting beam. We then come to the idea of guiding the slow electrons away from the beam by a toroidal magnetic field to preserve symmetry as much as possible in view of the wanted variability of parameters. In section 2 we will briefly discuss the traditional reaction microscope; in section 3 we present the concept for a reaction microscope in a storage ring and the simulation.

## 2. Traditional reaction microscopes

There are two main types of reaction microscopes in use [5], the transverse and the longitudinal reaction microscope, distinguished according to the direction of extraction relative to the projectile beam, shown in figure 1. The supersonic gas-jet target is intersected by a photon or ion beam, an appropriate electrostatic field is applied in the interaction region to separately direct the recoil ions and low energy electrons onto their two-dimensional position sensitive detectors, which are oriented transverse to the projectile direction. Space focusing can be accomplished by a simple electrostatic lens—generated by a step in the extraction field [6, 7]—focusing all ions with identical momenta but different starting positions in the plane defined by the ion and projectile directions onto the same position on the detector. Space focusing is, however, hardly ever used in reaction microscopes with magnetic fields. Time focusing geometry is used in almost all cases, which follows the rule that the drift length is approximately twice the extraction length, see [8, 9] for more details. With this spectrometer a resolution of 0.07 au FWHM for the recoil ion,

which is close to the internal temperature of the gas jet, has been achieved [8, 9].

However, an important class of collision experiments cannot be covered with the transverse geometry: fast electrons originating from projectile or target ionization processes such as ECC (non-radiative electron capture to the continuum), ELC (electron loss to the continuum), RECC (radiative electron capture to the continuum), appear as a prominent cusp at a velocity centred at the projectile velocity (that is, for instance, electrons with the energy of 2 keV arise for 3.6 AMeV beam specific energy), cannot be projected onto the electron detector. For this reason, for investigations of projectile ionization, of ECC, ELC, RECC, transfer ionization TI, (e, 2e) etc [5], another type of extraction has been developed, making the position-sensitive detection of fast forward emitted electrons possible.

Instead of extraction perpendicular to the projectile beam and the gas jet the ions can alternatively be extracted almost parallel to the projectile beam axis (figure 1(b)). This extraction geometry has been used at GSI [12] and Heidelberg [5]. In this extremely flexible spectrometer, the extraction field is generated by two parallel resistive plates. The magnitude and direction of the electric field can be easily adjusted and tuned by independently setting the potentials on the four corners of each plate. The gas jet intersects the reaction region through a hole in the centre of the upper and lower plates, respectively; the resulting distortion of the electric field is compensated by ring electrodes outside the hole on either plane [12].

The axis of the solenoidal magnetic field is conveniently set to have a small angle with the projectile beam of about  $8^\circ$ , such that the electrons are guided to the detector which is close to the right-hand side of the projectile beam. With a magnetic field of typically 10 Gauss all trajectories of electrons with transverse energies up to 100 eV are confined to a spiral with a maximum radius of 3.3 cm, independent of the longitudinal electric field strength; this makes a large solid angle of almost  $4\pi$  for electrons. Under these conditions the longitudinal and transverse momentum balances are decoupled and the respective components can be calculated from:

$$\vec{p}_\perp = 11.6 \cdot \frac{\vec{r} - \vec{r}_0}{2a + d} \cdot \sqrt{qU \cdot m} \quad (1)$$

$$\vec{p}_\parallel = 8.042 \times 10^{-3} \frac{qU}{a} (t_0 - t) \quad (2)$$

( $p$  in au,  $m$  in amu,  $qU$  in eV,  $a$  = length of acceleration distance and  $d$  = length of drift distance in cm,  $t - t_0$  is the electron flight time in ns).

In such a configuration, e.g.  $B = 10$  G, the cyclotron frequency for electrons  $\nu = \frac{1}{T} = \frac{eB}{2\pi m_e}$ , and the cycle  $T = \frac{2\pi m_e}{eB}$  is about 36 ns, thus the azimuth resolution is about  $10^\circ$ .

This configuration enables us to detect simultaneously the fast electrons emitted by the projectile into a narrow cone around the beam direction and all slow electrons for reasonable low collision energies of the projectiles when using multihit capable position sensitive electron detectors with associated electronics [5, 12]. Reasonable confinement can be achieved for fast forward electron kinetic energies not exceeding a few keV.

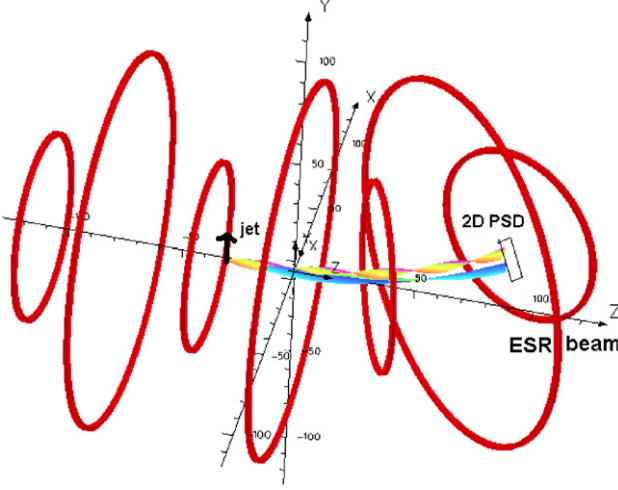


**Figure 2.** Arrangement of magnetic coils in the toroidal reaction microscope. The black arrow near the centre and the word ‘jet’ designate the location of the supersonic jet target. Two groups of trajectories extend from the jet target towards the 2D PSD. The lower group shows the trajectories of electrons with 10 eV as the transverse energy, and 2000 eV (fast electrons) as the longitudinal energy; in the simulations the electrons are emitted with azimuth from 0 to 350° every 10°, the velocity vectors form a cone. The other group contains electrons with the same condition except for 50 eV as longitudinal energy. Note that electrons with smaller longitudinal energies execute a noticeably larger number of cyclotron orbits than the faster electrons.

However, as the large electron detector (typical diameter 80 mm) is very close to the beam, when a large dynamic range of cross sections is to be measured and also in a storage ring environment, the energetic forward background electrons and background ions [19] are likely to blind the detector and thus prevent detection of electrons from low cross section reactions.

In an alternative approach to solve such problems of electron collection, two decades ago, by proper use of a magnetic field, P Kruit and co-workers generated a field parallelizer which is restricted to measure only very low energy electrons [18]. Through an inhomogeneous magnetic field, the electrons are parallelized with a maximum division of 1.8° (half angle).

### 3. Simulation for the toroidal reaction microscope

We describe here simulation calculations of a magnetic toroidal sector for electrons using OPERA-3d 10.5 [20]. OPERA-3d is the pre- and post-processor for well-known electromagnetic analysis programs including TOSCA, ELEKTRA, CARMEN, SOPRANO, TEMPO and SCALA. The magnetic field is calculated by TOSCA in our simulations; by solving the following partial differential equation with boundary conditions determined by the configuration of the experiment under consideration:

$$\nabla \cdot \mu \nabla \phi - \nabla \cdot \mu \left( \int_{\Omega_J} \frac{\mathbf{J} \times \mathbf{R}}{|\mathbf{R}|^3} d\Omega_J \right) = 0. \quad (3)$$

Here  $\mu$  is the permeability tensor, and  $\phi$  is the magnetic potential. The post-processor provides facilities for displaying the electromagnetic fields, and can calculate and plot particle trajectories through the calculated fields.

The geometric coordinates we used in the following figures are all as given in figure 2, if not specified. In the example configuration in figure 2, fast electrons are chosen with a forward energy 2 keV, corresponding to a specific energy of 3.6 AMeV for ions, along the beam direction and 10 eV transverse to the beam direction. In the simulations electrons are emitted with azimuth from 0 to 350° in steps of 10°, such that their velocity vectors form a cone around the beam direction; these electrons are projected onto the 2D detector. We simultaneously consider a group of slow electrons with 50 eV as the longitudinal energy and 10 eV as the transverse energy. They are all guided onto the 2D position-sensitive detector which is positioned 200 mm perpendicular distance from the coasting beam by the magnetic field generated by the coils.

The toroidal magnetic field is generated by seven coils of two groups; the bigger coils have a diameter of 160 cm, and the smaller coils have a diameter of 80 cm. This configuration allows the generation of a nearly constant field in the longitudinal section with  $\Delta B/B \leq 10^{-2}$ . The centres of the coils are arranged in a line along the beam axis followed by a toroidal sector of 60°, with 100 cm as the radius of curvature of the toroidal sector. In the present case, the magnetic fields generated are around 11 G. The magnitude of magnetic fields  $B$  along the centre of the coils as well as 2 cm around it in four directions are shown in figure 3, the left part curve (up to 0 on the abscissa) corresponding to the linear and the right part corresponding to the toroidal sector in figure 2. It is clearly seen that the toroidal magnetic  $B$  field differs from the solenoidal field in that  $B$  is asymmetric over the cross section of the coils, i.e., the closer to the centre of the toroidal sector (curve 4 in figure 3(a)), the higher the magnetic field is, as shown in the right part of figure 3(a), the inner curve (curve 4 which is closer to the centre of the toroidal sector) has a field of 11.1 G while the outer one (curve 1 which corresponds to a path at  $(-2, 0, 0)$  starting point, further away from the centre of the toroidal sector) of 10.8 G. The magnetic field in the sector plane is described by  $B(r) = \mu_0 I N / (2\pi r)$ , where  $r$  stands for the radius of curvature in the sector.

The positions of the electrons in figure 2 on the detector are shown in figure 4. The origin of  $X'$ ,  $Y'$  is at (20, 0, 60) in figure 2, i.e. at the centre of the 2D PSD electron detector;  $Y'$  is parallel to  $Y$  and  $X'$  is 37° with  $X$ . In the linear magnetic field, the longitudinal velocities of the electrons are always along the field direction, so that the electrons will follow exactly a helical motion according to  $F = qv \times B$ . However, in the toroidal magnetic field the longitudinal velocity always has an angle with the magnetic field, the electrons suffer a force downward which causes a drift to the  $-Y$  direction. As the direction of the magnetic field changes, the fast electrons are harder to guide; the fast electrons always have a resulting larger angle with the magnetic field, which causes the fast electrons to drift more than the slow electrons. Meanwhile the drift makes the motion of the electrons more complex. Finally, we see the positions of both fast and slow electrons on the detector plane, the slow electrons have drifted about 1 cm to  $-Y'$  and 4 cm to  $X'$  (the inner part of the toroidal sector), and the fast electrons have drifted 6 cm down to  $-Y'$  and 3 cm to  $X'$  (the inner part of the toroidal sector). We see here the time-of-flight of the fast electrons is close to a cyclotron cycle time, so that the electrons

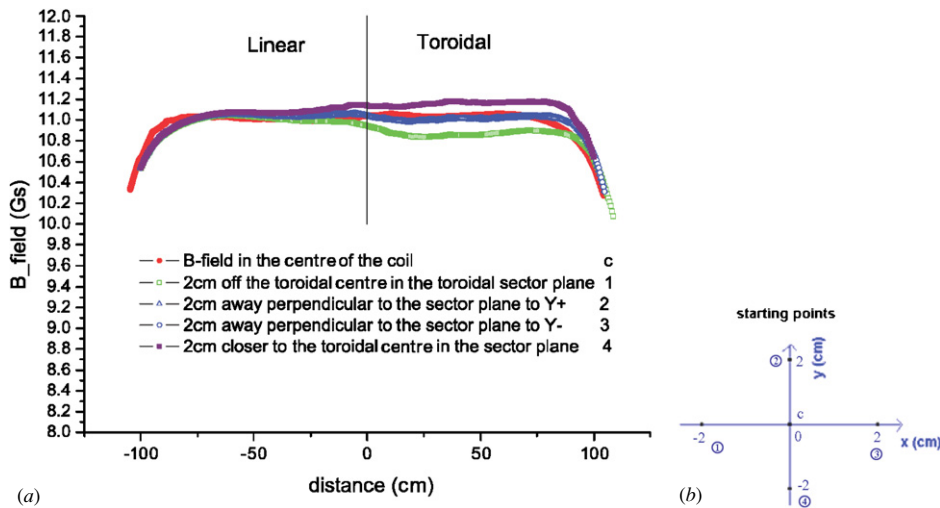


**Figure 3.** The magnitude of the magnetic field  $B$  generated by the coils. 0 is the reference point which separates the linear and toroidal parts; the distance is measured along the solenoidal and toroidal axis; the left part of the curve is for the linear part and the right part of the curve is for the toroidal sector. Curves 2 and 3 virtually coincide (blue in colour). For curve c the  $B$  field is along the centre of the coils and the other four curves start along  $x = \pm 2, y = \pm 2$  in the linear part. Note the zero suppression on the y scale.

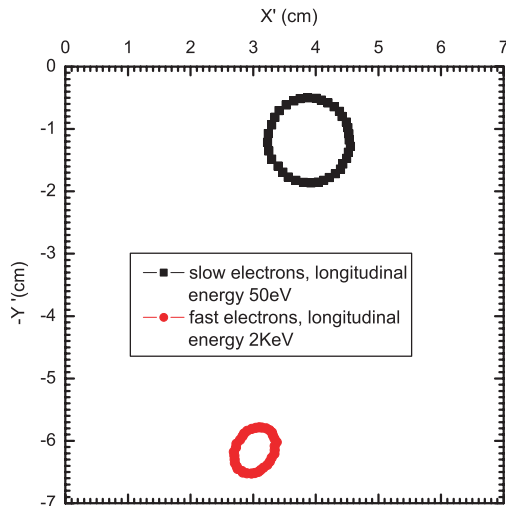


**Figure 4.** The positions of electrons in figure 2 on the detector plane. Both fast and slow electrons drift to  $-Y'$  and  $X'$ . The origin of  $X', Y'$  is at (13, 0, 50) in figure 2,  $Y'$  is parallel to  $Y$  and  $X'$  is  $30^\circ$  to  $X$ . The position of the beam in this figure is  $X' = -15.4, Y' = 0$ .

form a smaller circle. This can also be seen in the spirals of fast and slow electrons in figure 2.

### 3.1. Time-of-flight

In a linear (conventional) reaction microscope, the spiral motion frequency  $\omega = qB/m$  is independent of the azimuth. However, in the new toroidal geometry, as the electrons emitted from the same origin with different azimuth see different magnetic fields in the toroidal parts (or we can say that the  $B$ -field depends on the azimuth about the axis), the cyclotron frequency now as well is related to the azimuth of emission  $\omega(r) = qB(r)/m$ . Thus for electrons starting at the toroidal part, the graph of time-of-flight versus the distance from the centre in the toroidal part is shown in figure 5. Electrons

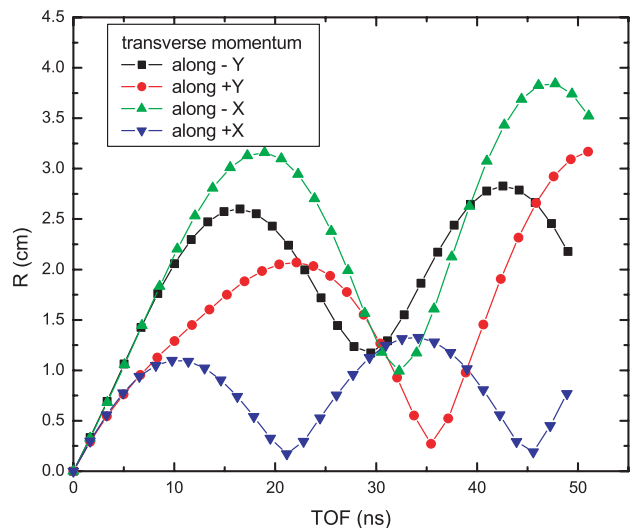


**Figure 5.** Electrons with 10 eV transverse and 200 eV longitudinal energies emitted to different azimuth (the transverse momentum along  $-Y, Y, -X, X$  respectively) from (0, 0, 0) in figure 2 to the toroidal part of the reaction microscope; compare with figure 8 in [2], in the toroidal case there is no universal  $T = \frac{2\pi m}{qB}$ , as  $B$  is  $r$ -dependent.

with 10 eV as transverse and 200 eV as longitudinal energy emitted into different azimuth angles from (0, 0, 0) in figure 2, see a different magnetic field, and so the cyclotron frequency is different for each starting direction; the four curves in figure 5 correspond to the transverse momentum along the four directions  $-Y, Y, -X, X$ , respectively. During the helical motion the field seen by the electron changes, the electron cannot go back to the axis  $r = 0$  as in the linear geometry (see figure 8 of [2]).

Additionally, the distance travelled along the outer part is longer than the corresponding distance along the inner part of the toroidal sector, thus the time-of-flight is also related to the

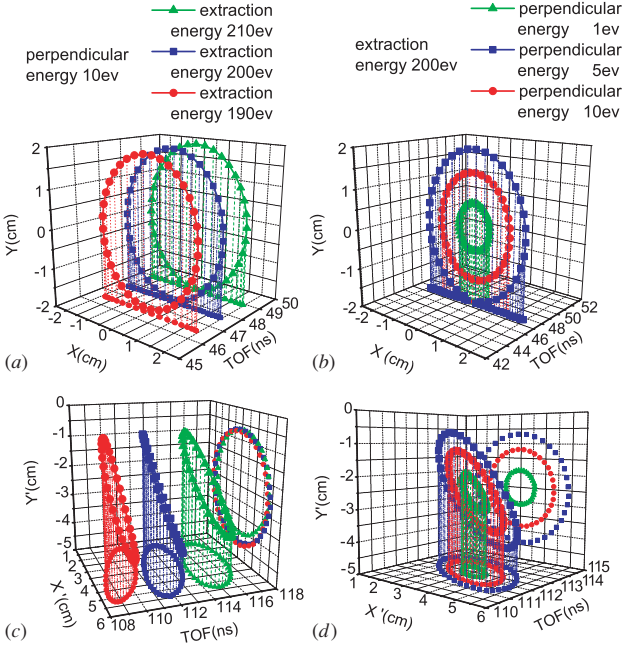


**Figure 6.** A linear reaction microscope electron branch and a toroidal reaction microscope electron branch are compared. Part (a) shows that for linear reaction microscopes, electrons with the same transverse energy have the same radius but different time-of-flight. Part (b) shows that for linear reaction microscopes, electrons with the same longitudinal energy result in the same time-of-flight, and different transverse energies lead to different radii. Part (c) shows that for the toroidal electron branch, the same initial condition in (b) leads to three ellipses in the (position–time) space, (d) shows that for the toroidal electron branch, the same condition in (b) leads to three circles on the same plane in the (position–time) space, the three groups having the same average time-of-flight.

azimuth of emission, which is quite different from the linear geometry. It thus appears that from a simple graph of only  $R =$  radial distance from axis interception on the detector versus time-of-flight no information like in the linear geometry (see figure 8 of [2]) can be derived.

For the position and time-of-flight information on the detector plane, figure 6 shows the comparison of the standard linear geometry with the new toroidal geometry. We will show that it is possible to reconstruct the initial momentum vectors in both configurations. The same  $X' Y'$  coordinates as in figure 4 are used. In a conventional reaction microscope, the longitudinal momentum (corresponding to the extraction energy) is derived from the time-of-flight of the electrons while the transverse momentum (corresponding to the perpendicular energy) is derived from the radius or the position on the detector, see equations (1) and (2), the TOF only have an effect on the phase. According to the calculation for the linear geometry with 10 eV as the transverse energy, and 200 eV as the longitudinal energy the electrons emitted with azimuth from 0 to 350° in steps of 10°, whose velocity vectors form a cone, are projected onto the detector, the time-of-flight and position information are shown in figures 6(a) and (b) (the blue rectangle). Figure 6(a) also shows the electrons with 10 eV as transverse energy but 210 eV and 190 eV as longitudinal energy. It is clearly seen that in a linear geometry, the same transverse energy leads to the same radius. Figure 6(c) shows the electron with 200 eV as longitudinal energy and 5 eV and

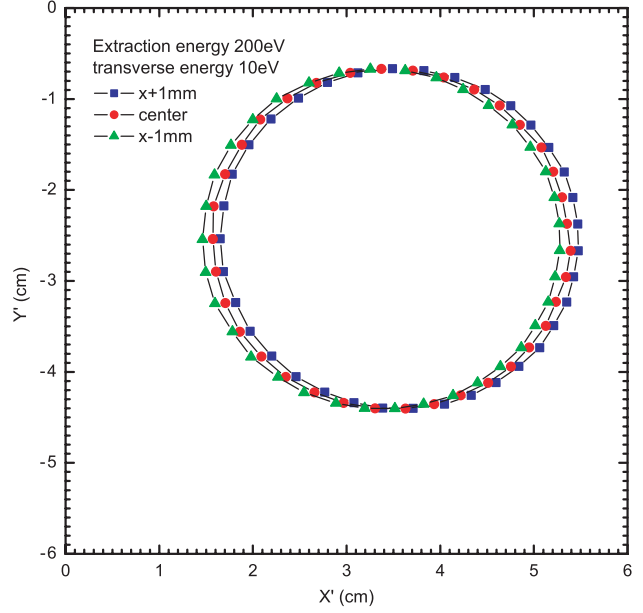


**Figure 7.** Electrons with 200 eV as extraction energy and 10 eV as transverse energy; as the starting point moves along the  $x$ -axis, the position has a drift towards the  $x'$  direction, which will slightly limit the energy resolution.

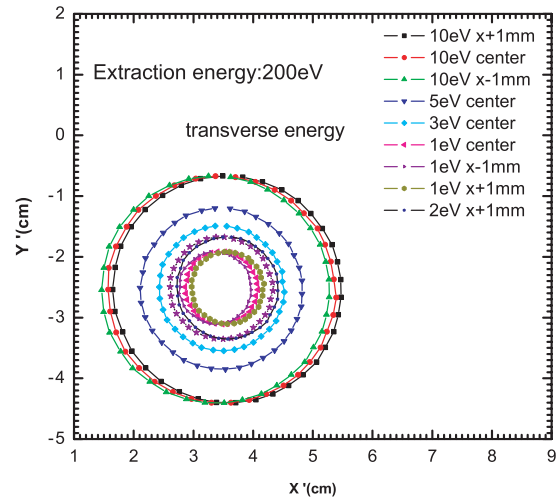


**Figure 8.** Simulations of the same type as in figure 7, with transverse energies of 10 eV, 5 eV, 3 eV, 2 eV and 1 eV, respectively.

1 eV as transverse energy. In the linear geometry, the same longitudinal energy always leads to the same time-of-flight. However, in a toroidal geometry, due to the asymmetry of toroidal magnetic field, the position information is coupled with the time-of-flight. Thus for toroidal geometry, electrons with the same initial conditions will have results as figures 6(c) and (d), the projected line in linear geometry in (position–time) space evolves into an ellipse in toroidal geometry. But still, the same time-of-flight in figure 6(b) leads to the same plane in figure 6(d) while the same radius in position of figure 6(a) leads to the same configuration in figure 6(c) but different average time-of-flight. The toroidal configuration still conserves the symmetry almost entirely. It is thus possible to reconstruct the initial momentum of the electron.

### 3.2. Resolution

For transverse momentum resolution, we estimated the resolution of electrons with 200 eV as extraction energy. We show here the effect of the target volume, as there is no space focusing in the toroidal configuration, the reaction volume, we see here as the starting point moves along the  $x$ -axis, the position has a drift to the  $x'$  direction; for the starting point moving along the  $y$ -axis, we have seen in the simulation a similar effect that the positions on the detector move along  $y'$  in the same direction.

With these kinds of simulations in figures 7 and 8, we can estimate that for a TOF resolving power of 1 ns and position resolving power of 0.2 mm, 1 eV can be resolved for electrons of 200 eV, which corresponds to a momentum resolution of about 0.3 au. In an experiment, of course, one deals in general with continua as primordial electron energy distributions and unfolding procedures will be implemented accordingly. A small prototype for a toroidal sector for the electron branch of a reaction microscope will be tested using Unilac beams, in GSI, Darmstadt.

### 4. Summary

We have presented simulation calculations using OPERA for a toroidal branch for electrons in a reaction microscope for experiments in ESR and NESR. We show that in spite of coupling of longitudinal and transverse momenta, the primordial momenta can be reconstructed.

### Acknowledgments

One of us (XW) acknowledges the kind hospitality extended to him by Professor J Kluge and his group at GSI during the course of this work.

### References

- [1] Gumberidze A *et al* 2005 *Phys. Rev. Lett.* **94** 223001
- [2] Wieman C and Hänsch T 1980 *Phys. Rev. A* **22** 192
- [3] Verdú J *et al* 2004 *Phys. Rev. Lett.* **92** 093002
- [4] Ali R *et al* 1992 *Phys. Rev. Lett.* **69** 2491
- [5] Ullrich J *et al* 2003 *Rep. Prog. Phys.* **66** 1463
- [6] Ullrich J *et al* 1997 *J. Phys. B: At. Mol. Opt. Phys.* **30** 2917
- [7] Doerner R *et al* 2000 *Phys. Rep.* **330** 95
- [8] Jagutzki O 1994 Entwicklung eines Rückstossionenimpulsspektrometers zur Untersuchung der Dynamik im Heliumatom *Dissertation* Universität Frankfurt
- [9] Mergel V 1996 Dynamische Elektronenkorrelationen in Helium, *Dissertation* Universität Frankfurt
- [10] Jardin P *et al* 1993 *HCI-5, AIP Conf. Proc.* **274** 291
- [11] Moshhammer R *et al* 1994 *Phys. Rev. Lett.* **73** 3371
- [12] Moshhammer R, Unverzagt M, Schmitt W, Ullrich J and Schmidt-Böcking H 1996 *Nucl. Instrum. Methods B* **108** 425
- [13] van Der Poel M *et al* 2001 *Phys. Rev. Lett.* **87** 123201-1
- [14] Turkstra J W *et al* 2001 *Phys. Rev. Lett.* **87** 123202-1
- [15] Flechard X *et al* 2001 *Phys. Rev. Lett.* **87** 123203-1
- [16] Bredy R *et al* 2003 *Nucl. Instrum. Methods B* **205** 191-5
- [17] Flechard X *et al* 2003 *Phys. Rev. Lett.* **91** 243005
- [18] Kruit P *et al* 1983 *J. Phys. E: Sci. Instrum.* **16** 313
- [19] Kozhuharov Ch 2006 Private communication
- [20] OPERA-3D User Guide, Vector Fields Limited, 24 Bankside, Kidlington, Oxford OX5 1JE, UK